2021 IEEE/RSJ International Conference on Intelligent Robots and Systems (IROS)
September 27 - October 1, 2021. Prague, Czech Republic

Human-Robot Collaboration for Heavy Object Manipulation: Kinesthetic Teaching of the Role of Wheeled Mobile Manipulator

Hongjun Xing[1,2], Ali Torabi[2], Liang Ding[1*], *Senior Member, IEEE*, Haibo Gao[1],
Weihua Li[1], Vivian K. Mushahwar[3], *Member, IEEE*, and Mahdi Tavakoli[2*], *Senior Member, IEEE*

***Abstract*— Human-robot collaboration (HRC) significantly extends robotic systems' applications when working in spaces like houses, hospitals, or laboratories. However, new challenges appear during a close collaboration between humans and robots and imitating the movement of humans by robots. Learning from demonstration (LfD), or kinesthetic teaching, is a popular approach to help teach a robot human behavior by demonstrations without the need to explicitly reprogram the robot for different procedures. In this paper, we propose a method for object manipulation, including lifting, carrying, and lowering the object through a collaboration of a human with a wheeled mobile manipulator (WMM). The WMM is first trained with the help of a human demonstrator to collaborate with the user to execute the task. Then, the WMM will independently cooperate with the user by reproducing the learned skills to perform the same task. The redundancy of the WMM will also be employed to enhance its force exertion capability in the vertical direction to offset the object's weight. The advantages and effectiveness of the proposed method are investigated through experiments.**

I. Introduction

Wheeled mobile manipulators (WMMs) have found many applications in diverse fields, including door opening for disaster rescue [1], heavy object pushing [2], and human-robot collaboration (HRC) [3] due to their mobility and manipulation capability. The addition of a mobile platform greatly enlarges a manipulator arm's workspace, enabling it to execute tasks requiring a large range of motion. Using WMMs for HRC is beneficial in improving work efficiency and reducing the human user's burden. Because the environment is unstructured and the tasks are unmodeled, taking full advantage of a WMM for HRC to execute tasks is incredibly challenging. Learning from Demonstration (LfD), or kinesthetic teaching, is a convenient and effective approach to teach a robot various skills through human demonstrations [4]. This approach considerably reduces the user's burden to program a complex robotic system and is also conducive to reproducing the desired human intention.

Averaged across all professions, the top cause of injury among workers is bodily reaction and exertion (including overexertion). One leading cause of overexertion is repetitive and demanding motions involving lifting and carrying heavy objects. Workers who perform repetitive tasks of loading and unloading risk injuries, musculoskeletal disorders, muscle fatigue, and low productivity. One way to avoid these injuries is by employing a WMM to offset the weight of the objects. Also, due to the impact of the COVID-19 pandemic, WMMs have found many applications to guarantee the safety of human users [5]. For the tasks that need two people to work together to carry an object, one of the workers can be replaced by a robot. In the demonstration phase for the LfD, the demonstrator will only need to be close to the user for a short time to reduce disease transmission risk.

The deployment of mobile manipulators in HRC has attracted many researchers in recent years [3], [6]–[9]. However, investigations to date have not considered the configuration optimization for the WMM to enhance its force exertion ability for heavy objects or employ the LfD technique to make the system "smarter". Also, the majority of the proposed methods only considered HRC in the horizontal motion in carrying the object; object lifting and lowering stages were not considered.

One limitation of the robotic system for HRC lies in that the system is not intelligent enough to understand the user's intention, but the LfD approach can solve this problem by intuitively transferring a human's knowledge of a task to a robot through demonstrations [10]. Learning based on the Gaussian mixture model (GMM) has become prominent in the fields related to HRC due to its need for only a few demonstrations, its lack of need for explicit programming on a task-specific basis, and fast computation compared with other learning methods, making it feasible for real-time implementation. From our group, Fong *et al.* utilized GMM to encode the task trajectory during the demonstration phase and realized impedance-based behavior learning through stiffness estimation [11]. Then, they performed motion reproduction via Gaussian mixture regression (GMR) [12] during the imitation phase for kinesthetic teaching of rehabilitation robots. Rozo *et al.* [10] put forward a task-parameterized version of GMM (TP-GMM) to encode the demonstrations

This research was supported by the Canada Foundation for Innovation (CFI), the Natural Sciences and Engineering Research Council (NSERC) of Canada, the Canadian Institutes of Health Research (CIHR), the Alberta Jobs, Economy and Innovation Ministry's Major Initiatives Fund to the Center for Autonomous Systems in Strengthening Future Communities, the National Natural Science Foundation of China (Grant No. 51822502, 51705096), the "111" Project (Grant No. B07018), and the China Scholarship Council under Grant [2019]06120165. (Liang Ding and Mahdi Tavakoli are the corresponding authors).

[1]H. Xing, L. Ding, H. Gao, and W. Li are with the State Key Laboratory of Robotics and System, Harbin Institute of Technology, Harbin 150001, China. {xinghj, liangding, gaohaibo, liweihua}@hit.edu.cn

[2]H. Xing, A. Torabi, and M. Tavakoli are with the Department of Electrical and Computer Engineering, University of Alberta, Edmonton T6G 1H9, Alberta, Canada. {ali.torabi, mahdi.tavakoli}@ualberta.ca

[3]V. Mushahwar is with the Department of Medicine, Division of Physical Medicine and Rehabilitation, University of Alberta, Edmonton T6G 2E1, Alberta, Canada Vivian.Mushahwar@ualberta.ca

and used GMR to reproduce the learned results. This method has been effectively implemented in human-robot cooperative transportation and assembly missions. However, the feasibility of the tasks has been significantly limited by the manipulator's workspace.

The exploitation of WMMs can ease the kinematic and dynamic limitations of robotic systems, which is another obstacle for HRC. For instance, the WMM has an unlimited workspace in the horizontal plane. Also, if the WMM system is redundant for a given task, which means there are more degrees of freedom (DOFs) in the system than the task needs, the redundancy of the robotic system can be used to enhance some required features for a task with null-space control. From our group, Torabi *et al.* [13], [14] used the redundancy of surgical robots to enhance the task performance for surgeons. Chen *et al.* [15] proposed a dexterous grasping method for a WMM to maximize its manipulability on a given manipulation task via null-space control. To improve the force exertion capability of a redundant manipulator, Chiu [16] provided the notion of task compatibility, which could strengthen the force exertion capability in a predefined direction. Ajoudani *et al.* [17] advanced this concept by introducing a joint torque scaling matrix to handle the difference among the joint torque limits. However, both approaches were only conducted with a single manipulator and not for a WMM system.

In the field of LfD for HRC, most of the literature only focuses on some simple tasks or a portion of a complex mission, such as moving an object [10] and handing over an object [18]. In terms of performing configuration optimization for a WMM system, most of the previous work has been limited to ensuring singularity avoidance and manipulability maximization [19]. These efforts failed to address the problem of limited force exertion capability of the robot, which may be needed during the execution of the object manipulation tasks if the object is heavy. For heavy object manipulation, the redundancy of the WMM system also has the potential to be implemented to enhance the system's force exertion capability in a required direction.

This study aims to present an approach to teaching a WMM from demonstrations to execute heavy object manipulation through the HRC framework. Large forces are prerequisites for manipulating a heavy object. Thus, in this study, we improve the WMM force exertion capability in a predefined direction by kinematic reconfiguration. The main contributions of the paper are as follows: (1) An HRC method for realizing heavy object manipulation (lifting, carrying, and lowering) with a WMM using the combination of Cartesian space motion learning and null-space optimization control is proposed; (2) for end-effector motion imitation, a stiffness estimation method based on the learned GMM to reproduce the demonstrator's impedance-based behavior to achieve the high-rigidity requirement in the vertical direction, and GMR to realize the compliant motion demand in the horizontal plane are adopted; and (3) a null-space reconfiguration optimization approach is provided to enhance the end-effector's force exertion capability in a predefined direction with consideration of the manipulator's gravity.

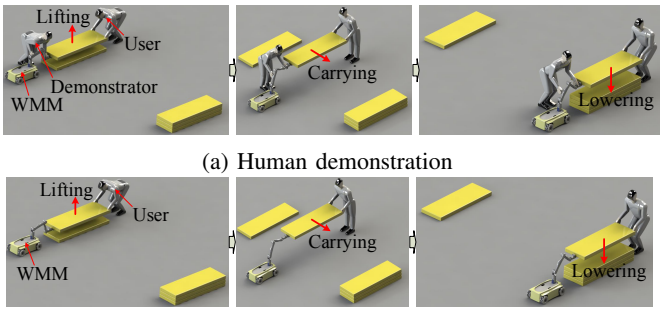

(a) Human demonstration

(b) Robot imitation

Fig. 1: Illustration of LfD procedure for object manipulation via HRC.

Fig. 1 shows the general diagram of manipulating an object using LfD in this paper, which can be divided into three stages: lifting, carrying, and lowering. Fig. 1a shows the demonstration phase, where a demonstrator/helper teaches the WMM how to handle the task with the user. The WMM will then learn the demonstrator's task skills and can subsequently complete the task independently with the user, as shown in Fig. 1b. The lifting and lowering stages contain sizeable force output in the vertical direction during movement. Thus, the interaction force between the human and the object should be learned in addition to the motion between them. The carrying phase involves only the desirable compliant movement in the horizontal plane. Therefore, only the kinematic motion will be learned and reproduced.

The remainder of this paper is organized as follows. Section II provides the kinematic modeling and compliance control method of WMMs. In Section III, the learning and reproduction approaches from human demonstration with HRC are presented. Experiments that illustrate the validity and advantages of the proposed approach are shown in Section IV. Section V summarizes the approach and its outcomes.

II. Kinematic Modeling and Compliance Control of WMMs

In this section, the forward kinematics at the velocity level for WMMs are presented. A Cartesian space admittance control scheme to achieve compliance and a null-space optimization algorithm to realize force exertion capability enhancement are also provided.

A. Kinematic Modeling of WMMs

The WMM in this study is composed of a manipulator arm mounted on a mobile platform. Thus, the kinematic model for the entire WMM system is derived based on the two subsystems' kinematic models – the mobile platform and the manipulator. With the assumption that there is no slippage or skidding between the wheels of the mobile platform and the ground (i.e., pure rolling), we can express the kinematic model of the mobile platform as $\dot{q}_p = G(q_p)v_p$, where

$\dot{q}_p \in \mathbb{R}^{n_p}$ represents the generalized coordinate vector of the mobile platform and $v_p \in \mathbb{R}^p$ is the input velocity vector of the wheels. $G(q_p) \in \mathbb{R}^{n_p \times p}$ denotes the constraint matrix of the platform (holonomic or nonholonomic) that transfers the wheel velocities to the generalized platform velocities. The manipulator is usually subject to holonomic constraints, i.e., its generalized velocity vector $\dot{q}_m \in \mathbb{R}^m$ can be assigned arbitrarily at any manipulator configuration. Here, we specify $\dot{q}_m = v_m$, where $v_m \in \mathbb{R}^m$ denotes the joint velocity input vector for the manipulator.

The generalized coordinate vector and velocity input vector for the entire WMM system are defined as $q = [q_p^{\mathrm{T}}, q_m^{\mathrm{T}}]^{\mathrm{T}} \in \mathbb{R}^{n_p+m}$ and $v = [v_p^{\mathrm{T}}, v_m^{\mathrm{T}}]^{\mathrm{T}} \in \mathbb{R}^n$, respectively, where $n = p + m$. Then, the forward kinematics at velocity level for the entire WMM can be calculated as

$$\begin{aligned} \dot{x} &= J_u(q)\dot{q} = [J_p(q) \quad J_m(q)] \begin{bmatrix} \dot{q}_p \\ \dot{q}_m \end{bmatrix} \\ &= [J_b(q)G(q_p) \quad J_m(q)] \begin{bmatrix} v_p \\ v_m \end{bmatrix} = J(q)v, \end{aligned} \tag{1}$$

where $\dot{x} \in \mathbb{R}^r$ is the Cartesian space velocity vector of the end-effector with its dimension being r, $J_p(q) \in \mathbb{R}^{r \times n_p}$ and $J_m(q) \in \mathbb{R}^{r \times m}$ denote the Jacobians of the mobile platform and the manipulator, respectively, $J_u(q) \in \mathbb{R}^{r \times (n_p+m)}$ represents the Jacobian of the unconstrained WMM, and $J(q) \in \mathbb{R}^{r \times n}$ represents the Jacobian of the WMM. It is noteworthy that there are two Jacobians for a WMM because the generalized velocity vector $\dot{q}_p$ for the mobile platform is not its wheel velocity inputs v_p.

B. Compliance Rendered by an Admittance Control Scheme

To achieve robot learning by human demonstration, the WMM should be compliant with the human or environment's external force. One approach is utilizing impedance control for a torque-controlled robotic system [10], [12], in which an accurate dynamic model for the system is required. However, this approach is not applicable for WMM systems since most of the mobile platforms are velocity-controlled, and the complex wheel-ground contact is hard to model if not impossible [20]. Instead, an admittance control scheme is adopted here with the transfer function at velocity level expressed as

$$\frac{\dot{x}_e(s)}{f_e(s)} = R(s) = \frac{s}{\Lambda s^2 + \Psi s + \Gamma}, \tag{2}$$

where s denotes the Laplace operator, $f_e \in \mathbb{R}^r$ denotes the external force vector, and $\dot{x}_e \in \mathbb{R}^r$ represents the resultant end-effector velocity vector. $\Lambda \in \mathbb{R}^{r \times r}$, $\Psi \in \mathbb{R}^{r \times r}$, and $\Gamma \in \mathbb{R}^{r \times r}$ are diagonal matrices representing the desired Cartesian inertial, damping, and stiffness, respectively. Then, the desired end-effector velocity is defined as $\dot{x}_d(t) = \dot{x}_e(t)$ to realize compliance. It is noteworthy that the end-effector force $f_e(t)$ is estimated by establishing a disturbance observer for the manipulator.

C. Null-space Control Scheme to Realize Force Enhancement

The WMM is usually a kinematically redundant system (i.e., $r < n$). Thus, for a reference end-effector velocity vector defined as $\dot{x}_r(t)$, the kinematic controller for the WMM with null-space control considered can be expressed as (the dependence of the variables upon the joint variables are omitted for brevity)

$$v_r = J^{\dagger}\dot{x}_r + (I - J^{\dagger}J)v_N, \tag{3}$$

where $v_r \in \mathbb{R}^n$ represents the reference WMM's joint velocity vector, $J^{\dagger} = W^{-1}J^{\mathrm{T}}(JW^{-1}J^{\mathrm{T}})^{-1}$ denotes the weighted pseudoinverse of J with W being a symmetric and positive-definite weighting matrix, I represents an $n \times n$ identity matrix, $I - J^{\dagger}J$ is the null-space of J, and $v_N \in \mathbb{R}^n$ is the null-space velocity vector for configuration optimization. To track a desired trajectory provided by both the desired end-effector position $x_d(t)$ and the desired end-effector velocity $\dot{x}_d(t)$, a closed-loop controller [2] can be employed to restate $\dot{x}_r$ in (3) as $\dot{x}_r(t) = \dot{x}_d(t) + K_x\big(x_d(t) - x(t)\big)$, where K_x is a constant gain scalar.

For heavy object manipulation tasks via HRC, the required force to counteract the object weight for the robotic system may be large. Due to the limited manipulator joint torque output, some heavy objects cannot be lifted. Hence, the null-space control is implemented in this work to enhance the end-effector force exertion capability via kinematic reconfiguration.

With consideration of the joint torque limits of the manipulator, a scalar cost function is defined as [17]

$$\sigma_1 = \left[u^{\mathrm{T}}(J_m W_\tau W_\tau J_m^{\mathrm{T}})u\right]^{-1} \tag{4}$$

to maximize the end-effector's force exertion ability in the predefined direction, where $u \in \mathbb{R}^r$ is a unit vector denoting the optimization direction. $W_\tau = \mathrm{diag}[\frac{1}{\tau_{m\lim_1}} \ \cdots \ \frac{1}{\tau_{m\lim_m}}]$ denotes a scaling matrix to normalize the joint torques with $\tau_{m\lim_i}$ being the torque limit of the i^{th} joint. However, the cost function in (4) does not include the manipulator gravity, which is configuration dependent. Thus, to maximize the force vector exerted only by the external force, another cost function is specified as

$$\sigma_2 = f_g^{\mathrm{T}} f_g / \alpha, \tag{5}$$

where $f_g = J_m^{-\mathrm{T}}\tau_g$ with $\tau_g \in \mathbb{R}^m$ being the joint torque vector caused by the manipulator gravity and α is a positive scalar gain, which makes targets σ_1 and σ_2 on the same order of magnitude. Combining (4) and (5), the cost function for the null-space controller can be defined as $\sigma = w_1\sigma_1 - w_2\sigma_2$, where w_1 and w_2 are two constant gains with $w_1 + w_2 = 1$. By calculating the partial derivative of σ to q_m, denoting as $\nabla_{q_m}\sigma$, we can obtain the null-space joint velocity vector for (3) as

$$v_N = k_N \begin{bmatrix} 0_{p\times 1} \\ (\nabla_{q_m}\sigma)^{\mathrm{T}} \end{bmatrix} \tag{6}$$

with k_N being a constant gain.

III. Learning and Reproduction of Collaboration Skills from Human Demonstrations

LfD is a method for a robotic system to learn and reproduce a human's desired behaviours from demonstration [12], [21]. In this section, we will focus on how to teach the WMM with the human's Cartesian space behaviour for heavy object manipulation through HRC. Also, the null-space control for force exertion capacity enhancement is employed as presented in Section II-C. Here, GMM is employed to encode the robot trajectory in the demonstration phase. In the lifting and lowering stages, the trained GMM and stiffness estimation technique are used to learn the demonstrator's impedance-based behavior; and in the carrying stage, the trained GMM and GMR are adopted to encode and reproduce the WMM position trajectory taught by the demonstrator.

A. Gaussian Mixture Model for Data Encoding

During the demonstration phase, the WMM and the demonstrator are holding one end of the heavy object. The WMM is made compliant via the admittance controller and completely controlled by the demonstrator. The other end of the object is grasped by the coagent to achieve the task. All the recorded data are divided into three portions corresponding to the three stages. For each stage, each demonstration $m \in \{1, 2, \cdots, M\}$ consists of $T_{i,m}$ datapoints creating a dataset of N_i datapoints $\{\xi_{i,n}\}_{n=1}^{N_i}$ with $N_i = \sum_{m=1}^{M} T_{i,m}$, where M represents the number of the demonstrations and $i = 1, 2, 3$ denotes the manipulation stage. Each $\xi_{i,n} \in \mathbb{R}^D$ is associated with the recorded data, including the end-effector position, velocity, and external force with D denoting the datapoint dimensionality.

Based on the demonstrations, the GMM is implemented to encode the data, presenting a probabilistic representation of the dynamics required to achieve the task. A GMM of $N_{k,i}$ components is expressed by a probability density function

$$p(\xi_{i,n}) = \sum_{k=1}^{N_{k,i}} p(k)p(\xi_{i,n}|k) \tag{7}$$

with $p(k) = \pi_{i,k}$ being the priors and $p(\xi_{i,n}|k)$ being the conditional density functions. In which, $\{\pi_{i,k}, \mu_{i,k}, \Sigma_{i,k}\}$ represent the parameters of the k^{th} Gaussian component of the i^{th} stage, denoting the prior probabilities, mean vectors, and covariance matrices, respectively.

The optimal estimation of the mixture parameters is carried out iteratively implementing the Expectation-Maximization (EM) algorithm until convergence [22] and k-means procedure is used to initialize the model parameters. For the k^{th} Gaussian component of the i^{th} stage, the E-step (expectation step) is expressed as

$$w_{i,n,k} = \frac{\pi_{i,k}\mathcal{N}(\xi_{i,n}|\mu_{i,k}, \Sigma_{i,k})}{\sum_{k}^{N_{k,i}} \pi_{i,k}\mathcal{N}(\xi_{i,n}|\mu_{i,k}, \Sigma_{i,k})}, \tag{8}$$

which plays an important role in deriving the stiffness of the virtual springs.

B. Demonstrator's Impedance-based Behavior Learning in Lifting and Lowering Stages

During the lifting and lowering stages of the task, the human and the robot should exert a sizeable force to neutralize the object's weight in the vertical direction. Here, we utilize several virtual spring models associated with each Gaussian component k to simulate the impedance-based behavior exerted by the demonstrator, which is expressed as

$$f_{s,i,n} = \sum_{k=1}^{N_{k,i}} w_{i,n,k}\big[K_{i,k}(\mu_{i,k}^{x} - x_{i,n})\big], \tag{9}$$

where $i = 1, 3$ indicates the lifting and lowering stages, $f_{s,i,n}$ is the demonstrator's force at step n, $K_{i,k}$ is a stiffness constant affiliated with the k^{th} Gaussian model, $\mu_{i,k}^{x}$ represents the positional component of the models' mean vectors $\mu_{i,k}$, and $x_{i,n}$ denotes the current end-effector position at step n.

Estimating the model stiffness in this paper is performed by implementing Least Squares (LS) estimation. After encoding the demonstration data via GMM, the observation matrix is defined as $\Phi_i = [\phi_{i,1}, \phi_{i,2}, \cdots, \phi_{i,N_i}]^{\mathrm{T}}$ with $\phi_{i,n} = \big[w_{i,n,1}(\mu_{i,1}^{x} - x_{i,n}), w_{i,n,2}(\mu_{i,2}^{x} - x_{i,n}), \cdots, w_{i,n,N_{k,i}}(\mu_{i,N_{k,i}}^{x} - x_{i,n})\big]$ using (8), and the demonstrator's force vector is denoted as $F_{s,i} = [f_{s,i,1}, f_{s,i,2}, \cdots, f_{s,i,N_i}]^{\mathrm{T}}$. Then, the unknown stiffness vector $K_i = [K_{i,1}, K_{i,2}, \cdots, K_{i,N_{k,i}}]^{\mathrm{T}}$ for all $N_{k,i}$ Gaussian models of the i^{th} stage can be expressed as

$$K_i = (\Phi_i^{\mathrm{T}}\Phi_i)^{-1}\Phi_i^{\mathrm{T}}F_{s,i}. \tag{10}$$

Combined with (10), during the reproduction phase, the estimated demonstrator's force $f_{est,i,n}$ can be generated using (9) with the current end-effector's position.

C. Gaussian Mixture Regression for Trajectory Learning in the Carrying Stage

During the carrying stage, the heavy object will be moved in the horizontal plane to the predefined destination, and no extra force is required in the plane. Thus, only the kinematic model of this stage will be learned and reproduced using the demonstrations. With the GMM representation in Section III-A, the reproduction of the movement in horizontal plane can be formulated as a regression problem using GMR [10]. The GMR model can retrieve the next actions on-the-fly relying on the Gaussian conditioning theorem and linear combination properties of Gaussian distributions.

In conventional GMR, the query points are defined as temporal values ξ_t, and the corresponding spatial values $\hat{\xi}_s$ can then be estimated via regression. For the k^{th} Gaussian component in the GMM of the second stage, the mean vector and covariance matrix with consideration of input and output parameters are expressed as [23]

$$\mu_{2,k} = \{\mu_{2,t,k}, \mu_{2,s,k}\},\ \Sigma_{2,k} = \begin{pmatrix} \Sigma_{2,t,k} & \Sigma_{2,ts,k} \\ \Sigma_{2,st,k} & \Sigma_{2,s,k} \end{pmatrix}, \tag{11}$$

respectively.

In this stage, the query points are defined as the time-independent end-effector positions, and the corresponding

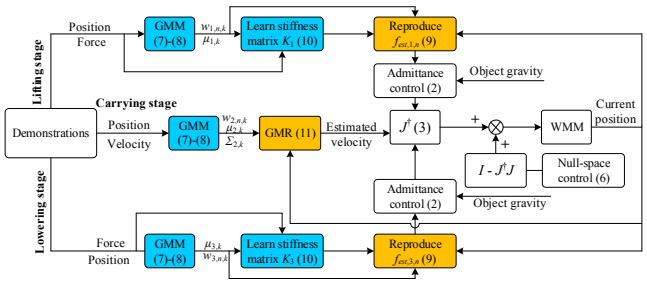

Fig. 2: Block diagram of the control system. The blue blocks denote the training system and the golden blocks represent the reproduction system.

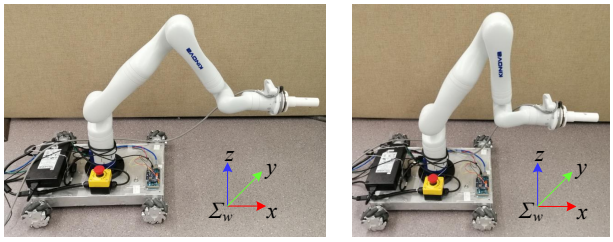

(a) Initial configuration (b) Final configuration

Fig. 3: Initial and final WMM configurations with null-space control. Σ_w denotes the world frame.

estimated parameters are the end-effector velocities. Thus, the demonstrator's behavior can be effectively imitated. The block diagram of the control system for object manipulation is illustrated in Fig. 2.

IV. Experimental Setup and Results

Several experiments were conducted to demonstrate the effectiveness of the proposed approach with a four-wheel omnidirectional mobile manipulator. The experimental demonstration contains two portions: (A) the verification of the force exertion capability enhancement approach via null-space control and (B) the validation of the human-robot collaboration for object manipulation using the LfD approach.

A. Experimental Setup

The experimental setup contains an omnidirectional wheeled mobile manipulator and an Axia80-ZC22 F/T sensor (ATI Industrial Automation, Apex, NC, USA). The WMM comprises a custom-built mobile platform and a 7-DOF ultra-lightweight robotic arm Kinova Gen3 (Kinova Robotics, Canada). The F/T sensor is employed to obtain the object weight exerted on the WMM.

The Cartesian space dimension for the mobile manipulator is defined to be $r = 6$ considering both the position and orientation of the end-effector. Yet, only the position compliance is treated, and for the orientation, a simple PD controller is employed to maintain it fixed. The initial joint position of the WMM is $v_0 = [0, 0, 0, 0, 0, 44°, 0, 101°, 0, -55°, 0]^{\mathrm{T}}$, where the first four values are the joints' position for the mobile platform. Thus, the end-effector's starting position is $x_0 = [0.640, -0.025, 0.332]^{\mathrm{T}}$ m using the system forward kinematics. The joint torque limit vector is defined as $\tau_{m\,\mathrm{lim}} = [40, 40, 40, 40, 16, 16, 16]^{\mathrm{T}}$ Nm for the manipulator.

B. Experiment on Force Exertion Capability Enhancement in Vertical Direction

For heavy object manipulation, some weighty items may not be lifted due to the bounded joint torque output. With the implementation of a WMM, its redundancy can augment the system's force exertion capability in the vertical direction. It is noteworthy that this procedure is only for the null-space control to obtain an optimal WMM configuration (without changing the end-effector pose).

The control parameters in this experiment are set as $K_x = 50$, $W_\tau = \mathrm{diag}(1, 1, 1, 1, 2.5, 2.5, 2.5)$, $k_N = 0.07$, $u = [0, 0, 1]^{\mathrm{T}}$, $\alpha = 600$, $w_1 = 0.6$, and $w_2 = 0.4$. The evolution of the WMM configuration is shown in the attached video, and the initial and final WMM configurations are shown in Fig. 3. The optimal WMM configuration for augmenting its load-carrying capability is shown in Fig. 3b. This is similar to how humans change their configuration to resist disturbance from the vertical direction.

The load-carrying ability of the WMM is compared in the two configurations that are depicted in Fig. 3 by adding known payloads to its end-effector. The results are shown in Fig. 4. During the experiment, first, a payload of 1 kg was added; and then, a weight of 3 kg was applied. Fig. 4a shows the manipulator joint torque output with the initial WMM configuration. When the 1 kg payload was added during time 5.40 – 21.05 s, all the joints could normally work with the maximal joint torque output being 35.31 Nm (joint 2). However, when the 3 kg weight was applied at time 31.38 s, the task stopped at 32.5 s due to the saturation of joint 2.

The joint torque output with the final WMM configuration is shown in Fig. 4b. With the 1 kg weight added during time 3.35 – 22.25 s, the joint with maximal torque output was joint 2, and the output was 26.24 Nm. When the payload of 3 kg was applied during time 34.70 – 54.90 s, the WMM with this configuration could also hold it, with the maximal joint output being 37.22 Nm (joint 2).

The joint torque increment caused by the end-effector force is investigated with a definition of weighted joint torque $\|\tau_{mw}\|_2 = \sqrt{\frac{\sum_{i=1}^{7} W_{\tau_i} \tau_{e_i}^2}{\sum_{i=1}^{7} W_{\tau_i}}}$, where W_{τ_i} denotes the i^{th} diagonal element of W_τ and τ_{e_i} represents the torque of the i^{th} manipulator joint caused by the external force. When the payload of 1 kg was applied, with the proposed method, the weighted joint torque was reduced from 1.182 Nm to 0.869 Nm, about 26.5% of its previous value. And with the 3 kg weight added on the WMM with the final configuration, the weighted joint torque was 2.559 Nm. These experimental results have illustrated the effectiveness of the proposed method in augmenting the force exertion ability for the end-effector.

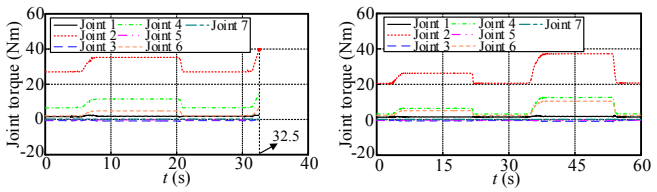

(a) Initial configuration (b) Final configuration

Fig. 4: Manipulator joint torque with two configurations.

C. Experiment on Human-Robot Collaboration for Object Manipulation with LfD

The final WMM configuration in Section IV-B is employed to conduct this section's experiment, and the null-space control is also utilized here. It is worth mentioning that the configuration optimization result in this experiment is not shown since it is already proved in Section IV-B. In this experiment, we select three objects with 1 kg, 3 kg, and 5 kg to demonstrate the performance of the LfD method in object manipulation. Here, two participants were involved, one human demonstrator and one human user.

During the demonstration phase, the WMM was admittance-controlled to follow the human demonstrator to complete the object manipulation task with the user. The desired Cartesian impedance parameters for the WMM system were defined as $\Lambda = \text{diag}(100, 100, 200)\,\text{Ns}^2/\text{m}$, $\Psi = \text{diag}(200, 200, 400)\,\text{Ns/m}$, and $\Gamma = \text{diag}(0, 0, 0)\,\text{N/m}$. The desired Cartesian impedance parameter Γ was set as zero to ensure that the robotic system could be led by the demonstrator smoothly.

For each object, four demonstrations were conducted, and some pictures of the demonstration phase are shown in Figs. 5a. The object's mass could be changed by adding or removing some known payloads to simulate manipulating different objects.

Due to the limitation of the paper length, only the WMM trajectory and demonstrator's force in the vertical direction in 5 kg scenario are shown in Fig. 6. During the demonstrations, the average motion distances of the WMM in [x, y, z] are [0.908, -1.395, 0.167] m, [0.978, -1.412, 0.165] m, and [1.013, -1.412, 0.157] m for 1 kg, 3 kg, and 5 kg payloads, where the corresponding stable support forces are approximately 4.92 N, 12.32 N, and 18.39 N, respectively.

Then, we manually divided each demonstration data into three stages: lifting, carrying, and lowering to perform data encoding using GMM. Three models of ten components ($N_{k,1} = 10$), twelve components ($N_{k,2} = 12$), and ten components ($N_{k,3} = 10$) were selected to train the three stages with the obtained demonstrations. Here, we will present the training results for the 1 kg scenario.

Fig. 7 shows the learning results for the lifting and lowering stages. In the lifting stage (Fig. 7a), the demonstrator force should be big enough to help the WMM lift the object with the user, while in the lowering stage (Fig. 7b), the force was smaller due to the object gravity. The *bottom row* of Fig. 7 presents the corresponding weighting matrices, which play

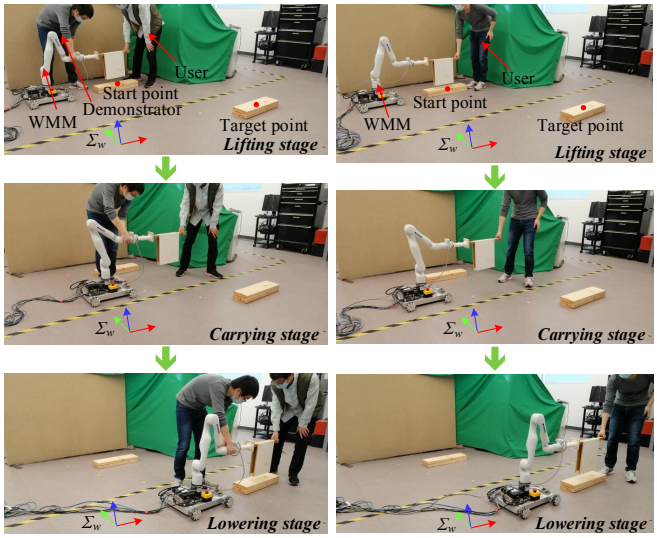

(a) Demonstration phase (b) Reproduction phase

Fig. 5: Pictures of demonstration and reproduction phases for object manipulation via HRC.

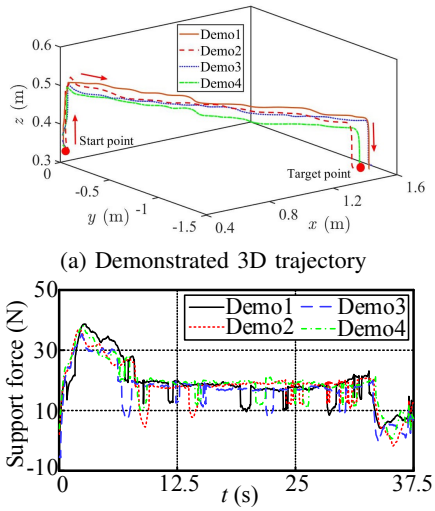

(a) Demonstrated 3D trajectory

(b) Support force

Fig. 6: Human demonstration for object manipulation with a 5 kg payload.

an essential role in imitating the demonstrator's impedance in the reproduction phase. The learned models of the x axis and y axis in the carrying stage are presented in Fig. 8, where the trained center and covariance matrix of each Gaussian model will be employed to derive the end-effector's velocity according to its corresponding position via GMR.

In the reproduction phase, the WMM cooperates with the user to conduct the object manipulation task using the learned demonstrator's skills. Here, the admittance control is only implemented in the vertical direction during the lifting and lowering stages. The moment for stage switching is detected when the end-effector reaches the corresponding targets, or the number of iterations outstretches the demonstration samples' length. Some snapshots of the reproduction procedure

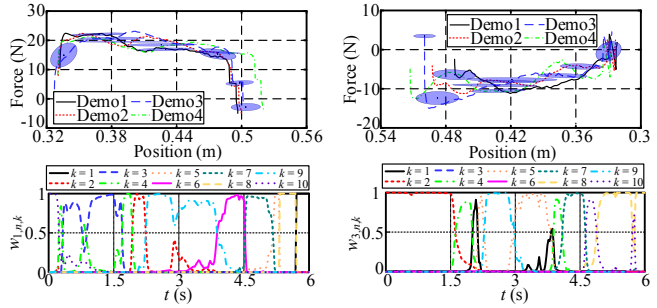

(a) Lifting stage (b) Lowering stage

Fig. 7: Model learning for lifting and lowering stages in 1 kg scenario. *Top row* shows the learned GMM and *bottom row* presents the corresponding model weights for demonstrator's impedance imitation.

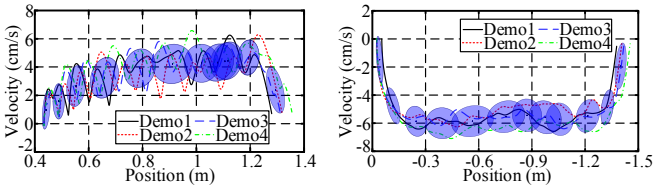

(a) x trajectory learning (b) y trajectory learning

Fig. 8: Model learning for carrying stage in 1 kg scenario.

are presented in Fig. 5b.

According to the demonstration data, we define the motion target for the lifting and lowering stages as 16 cm, and for the x and y in the carrying stage as 0.9 m and -1.35 m, respectively, in all the three scenarios. The end-effector trajectories for the reproduction experiment are shown in Fig. 9. The learning results of the demonstrator's impedance in the lifting and lowering stages are presented in Fig. 10, and the position-velocity profiles (resulting from GMR) for x and y in the carrying stage are provided in Fig. 11.

From Fig. 9, it is obvious that in the reproduction phase, the WMM can cooperate with the user to conduct the object manipulation task. In scenarios of 1 kg and 3 kg, the object

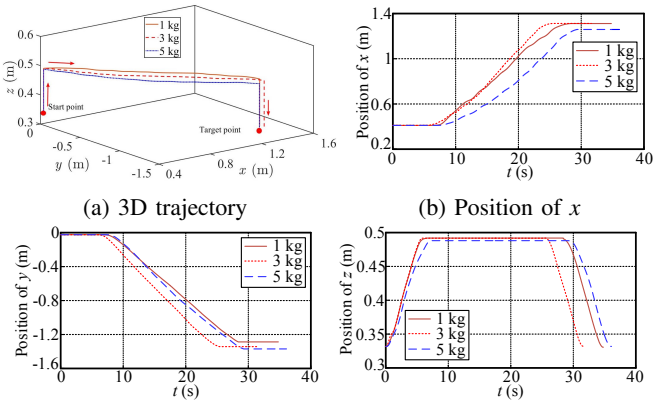

(a) 3D trajectory (b) Position of x

(c) Position of y (d) Position of z

Fig. 9: End-effector trajectory in the reproduction phase.

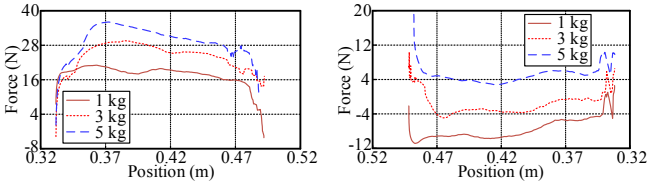

(a) Lifting stage (b) Lowering stage

Fig. 10: Reproduction results of the demonstrator's impedance-based behavior.

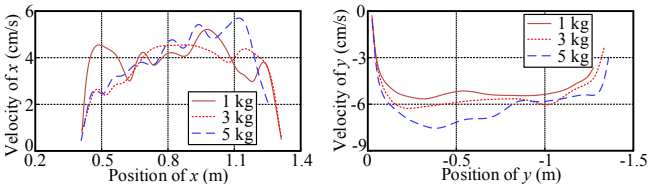

(a) Reproduction of x trajectory (b) Reproduction of y trajectory

Fig. 11: Reproduction of the horizontal trajectory in the carrying stage using GMR.

could be lifted 16 cm as we expected, and the desired horizontal displacement in x reached 0.9 m. However, the displacements in y only arrived at 1.26 m and 1.31 m for 1 kg and 3 kg payloads, respectively. In the scenario of 5 kg, the motion displacement for x and z were 0.848 m and 15.6 cm, but the destination in y was reached.

The reproduction results for the demonstrator's force and the horizontal velocity in Figs. 10 and 11 are similar to the results in the demonstration phase. The maximum of the mean absolute error (MAE) for the reproduced demonstrator's force to the mean of those gained in the demonstrations appears in the lifting stage of the 5 kg scenario, about 2.84 N, accounting for 8.35% of the maximal support force. The maximum of the MAE for the reproduced horizontal velocity is found to be approximately 0.57 cm/s in the x direction of the 1 kg scenario, representing 12.1% of the maximal commanded velocity in the corresponding direction. Both the WMM trajectory and the reproduction results illustrate the effectiveness of the proposed method in helping a user perform object manipulation tasks.

V. Conclusions

In this paper, an approach for realizing heavy object manipulation with human-robot collaboration via learning from demonstration (LfD) is provided. The redundancy of the wheeled mobile manipulator (WMM) system is employed to enhance the end-effector's force exertion ability along the vertical direction to facilitate the carrying and transport of heavy objects. The WMM is first admittance-controlled to follow the demonstrator to conduct the object manipulation task with the user. The obtained demonstrations are then manually divided into three stages: lifting, carrying, and lowering for training. Gaussian mixture model (GMM) and a stiffness estimation technique are adopted to learn

the demonstrator's impedance behavior in the lifting and lowering stages. GMM and Gaussian mixture regression are implemented to reproduce the WMM motion in the carrying stage. The effectiveness of the proposed approach has been experimentally verified with a 4-wheel mobile manipulator. For force exertion capability enhancement, the weighted joint torque for a 1 kg payload was reduced by 26.5% using the proposed method. For object manipulation, three loads with different masses have been tested via LfD, and the results show that the reproduction error is no more than 7% of the desired value. Our future work will focus on improving the learning algorithm to establish a unified control framework to conduct complex tasks, how to detect and react to unexpected conditions in the reproduction phase, and how to include vision to determine the goal location.

REFERENCES

[1] H. Xing, K. Xia, L. Ding, H. Gao, G. Liu, and Z. Deng, "Unknown geometrical constraints estimation and trajectory planning for robotic door-opening task with visual teleoperation assists," *Assembly Automation*, vol. 39, no. 3, pp. 479–488, 2019.

[2] H. Xing, A. Torabi, L. Ding, H. Gao, Z. Deng, and M. Tavakoli, "Enhancement of force exertion capability of a mobile manipulator by kinematic reconfiguration," *IEEE Robotics and Automation Letters*, vol. 5, no. 4, pp. 5842–5849, 2020.

[3] A. Mörtl, M. Lawitzky, A. Kucukyilmaz, M. Sezgin, C. Basdogan, and S. Hirche, "The role of roles: Physical cooperation between humans and robots," *The International Journal of Robotics Research*, vol. 31, no. 13, pp. 1656–1674, 2012.

[4] Y. Huang, J. Silvério, L. Rozo, and D. G. Caldwell, "Hybrid probabilistic trajectory optimization using null-space exploration," in *2018 IEEE International Conference on Robotics and Automation (ICRA)*. IEEE, 2018, pp. 7226–7232.

[5] M. Tavakoli, J. Carriere, and A. Torabi, "Robotics, smart wearable technologies, and autonomous intelligent systems for healthcare during the COVID-19 pandemic: An analysis of the state of the art and future vision," *Advanced Intelligent Systems*, p. 2000071, 2020.

[6] M. Lawitzky, A. Mörtl, and S. Hirche, "Load sharing in human-robot cooperative manipulation," in *19th International Symposium in Robot and Human Interactive Communication*. IEEE, 2010, pp. 185–191.

[7] D. Ćehajić, S. Hirche *et al.*, "Estimating unknown object dynamics in human-robot manipulation tasks," in *2017 IEEE International Conference on Robotics and Automation (ICRA)*. IEEE, 2017, pp. 1730–1737.

[8] Y. Jia, H. Wang, P. Stürmer, and N. Xi, "Human/robot interaction for human support system by using a mobile manipulator," in *2010 IEEE International Conference on Robotics and Biomimetics*. IEEE, 2010, pp. 190–195.

[9] B. Navarro, A. Cherubini, A. Fonte, G. Poisson, and P. Fraisse, "A framework for intuitive collaboration with a mobile manipulator," in *2017 IEEE/RSJ International Conference on Intelligent Robots and Systems (IROS)*. IEEE, 2017, pp. 6293–6298.

[10] L. Rozo, S. Calinon, D. G. Caldwell, P. Jimenez, and C. Torras, "Learning physical collaborative robot behaviors from human demonstrations," *IEEE Transactions on Robotics*, vol. 32, no. 3, pp. 513–527, 2016.

[11] J. Fong and M. Tavakoli, "Kinesthetic teaching of a therapist's behavior to a rehabilitation robot," in *2018 International Symposium on Medical Robotics (ISMR)*. IEEE, 2018, pp. 1–6.

[12] J. Fong, C. Martinez, and M. Tavakoli, "Ways to learn a therapist's patient-specific intervention: Robotics-vs telerobotics-mediated hands-on teaching," in *2019 International Conference on Robotics and Automation (ICRA)*. IEEE, 2019, pp. 870–876.

[13] A. Torabi, M. Khadem, K. Zareinia, G. R. Sutherland, and M. Tavakoli, "Application of a redundant haptic interface in enhancing soft-tissue stiffness discrimination," *IEEE Robotics and Automation Letters*, vol. 4, no. 2, pp. 1037–1044, 2019.

[14] A. Torabi, K. Zareinia, G. R. Sutherland, and M. Tavakoli, "Dynamic reconfiguration of redundant haptic interfaces for rendering soft and hard contacts," *IEEE Transactions on Haptics*, pp. 1–1, 2020.

[15] F. Chen, M. Selvaggio, and D. G. Caldwell, "Dexterous grasping by manipulability selection for mobile manipulator with visual guidance," *IEEE Transactions on Industrial Informatics*, vol. 15, no. 2, pp. 1202–1210, 2019.

[16] S. L. Chiu, "Task compatibility of manipulator postures," *The International Journal of Robotics Research*, vol. 7, no. 5, pp. 13–21, 1988.

[17] A. Ajoudani, N. G. Tsagarakis, and A. Bicchi, "Choosing poses for force and stiffness control," *IEEE Transactions on Robotics*, vol. 33, no. 6, pp. 1483–1490, 2017.

[18] H. Admoni, A. Dragan, S. S. Srinivasa, and B. Scassellati, "Deliberate delays during robot-to-human handovers improve compliance with gaze communication," in *Proceedings of the 2014 ACM/IEEE international conference on Human-robot interaction*, 2014, pp. 49–56.

[19] H. Zhang, Y. Jia, and N. Xi, "Sensor-based redundancy resolution for a nonholonomic mobile manipulator," in *2012 IEEE/RSJ International Conference on Intelligent Robots and Systems*. IEEE, 2012, pp. 5327–5332.

[20] H. Xing, A. Torabi, L. Ding, H. Gao, Z. Deng, V. K. Mushahwar, and M. Tavakoli, "An admittance-controlled wheeled mobile manipulator for mobility assistance: Human–robot interaction estimation and redundancy resolution for enhanced force exertion ability," *Mechatronics*, vol. 74, p. 102497, 2021.

[21] B. D. Argall, S. Chernova, M. Veloso, and B. Browning, "A survey of robot learning from demonstration," *Robotics and autonomous systems*, vol. 57, no. 5, pp. 469–483, 2009.

[22] L. Rozo Castañeda, S. Calinon, D. Caldwell, P. Jimenez Schlegl, and C. Torras, "Learning collaborative impedance-based robot behaviors," in *Proceedings of the twenty-seventh AAAI conference on artificial intelligence*, 2013, pp. 1422–1428.

[23] S. Calinon, F. Guenter, and A. Billard, "On learning, representing, and generalizing a task in a humanoid robot," *IEEE Transactions on Systems, Man, and Cybernetics, Part B (Cybernetics)*, vol. 37, no. 2, pp. 286–298, 2007.